ADVANCED FUNCTIONAL MATERIALS
www.afm-journal.de

An Extremely Stable, Highly Soluble Monosubstituted Anthraquinone for Aqueous Redox Flow Batteries

Kiana Amini, Emily F. Kerr, Thomas Y. George, Abdulrahman M. Alfaraidi, Yan Jing, Tatsuhiro Tsukamoto, Roy G. Gordon, and Michael J. Aziz**

An extremely stable, energy-dense (53.6 Ah L^{-1}, 2 M transferrable electrons), low crossover (permeability of $<1 \times 10^{-13}$ cm^2 s^{-1} using Nafion 212 (Nafion is a trademark polymer from DuPont)), and potentially inexpensive anthraquinone with 2-2-propionate ether anthraquinone structure (abbreviated 2-2PEAQ) is synthesized and extensively evaluated under practically relevant conditions for use in the negolyte of an aqueous redox flow battery. 2-2PEAQ shows a high stability with a fade rate of 0.03–0.05% per day at different applied current densities, cut-off voltage windows, and concentrations (0.1 and 1.0 M) in both a full cell paired with a ferro/ferricyanide posolyte as well as a symmetric cell. 2-2PEAQ is further shown to have extreme long-term stability, losing only ≈0.01% per day when an electrochemical rejuvenation strategy is employed. From post-mortem analysis (nuclear magnetic resonance (NMR), liquid chromatography–mass spectrometry (LC-MS), and cyclic voltammetry (CV)) two degradation mechanisms are deduced: side chain loss and anthrone formation. 2-2PEAQ with the ether linkages attached on carbons non-adjacent to the central ring is found to have three times lower fade rate compared to its isomer with ether linkages on the carbon adjacent to the central quinone ring. The present study introduces a viable negolyte candidate for grid-scale aqueous organic redox flow batteries.

1. Introduction

Development of reliable energy storage technologies is a critical step for resolving the intermittency problem of renewable sources of energy and for their extensive penetration into the electrical grid.[1,2] Redox flow batteries (RFBs) are large-scale storage technologies that are attractive due to their flexible design, safety, and long life.[3] In RFBs, two separate reservoirs store electrolytes externally from the battery cell components. The electrolytes are commonly aqueous solutions containing redox active species. During the charge/discharge cycles, the electrolytes are continuously pumped into the cell to allow the electrochemical reactions to occur inside the cell. This modular architecture of RFBs permits the independent scale up and optimization of energy and power capacities of the battery.[4]

To date, the most studied and manufactured RFB technology has been based on vanadium chemistry at its four oxidation states.[5] Nevertheless, vanadium RFBs suffer from crossover problems during the operation, necessitating the use of rebalancing systems.[6] Additionally, the volatile cost of vanadium metal adds another layer of difficulty to their commercialization.[7] Hence, there has been great interest in the development of alternative redox active species from inexpensive precursors, with high solubility, good stability, and low crossover.[8] Among different types of electroactive species studied to date, organic-based compounds are attractive due to the possibility of tuning their electrochemical properties.[9–11] To date, organic species based on core structures of quinones,[9] ferrocenes,[12,13] viologens,[14,15] phenazines,[16,17] and alloxazines[18] have been explored.[19] Among these reported studies, anthraquinones such as 2,6-DPPEAQ,[20] DPivOHAQ,[21] DBAQ,[21] 2,6-NTSAQ,[22] AQDP,[23] and DCDHAQ[24] with demonstrated[9] fade rates <0.03% per day at maximum demonstrated concentration of 0.5–0.75 M have been reported. At the higher end of demonstrated concentrations, AQ-1,8-3E-OH[25] is reported to have a large fade rate of 0.5% per day when tested at 1.5 M. Hence, development of negolyte candidates with combined advantage of high stability and high solubility is extremely important for commercialization of organic-based RFBs.

It is highly preferable to have a smaller molecular weight (MW) per mole transferrable electrons in species that can be synthesized via simple synthesis routes because both of these attributes correlate with low mass production cost. While complicated synthesis routes and chemical structures are attractive for exploratory research to push the performance envelope, the more important challenge has become the development of low-MW redox active molecules with simple synthesis routes that can nevertheless deliver very good performance. In this work, we present 2-2-propionate ether anthraquinone

K. Amini, T. Y. George, A. M. Alfaraidi, M. J. Aziz
Harvard John A. Paulson School of Engineering and Applied Sciences
29 Oxford Street, Cambridge, MA 02138, USA
E-mail: maziz@harvard.edu
E. F. Kerr, Y. Jing, T. Tsukamoto, R. G. Gordon
Department of Chemistry and Chemical Biology
Harvard University
12 Oxford Street, Cambridge, MA 02138, USA
E-mail: gordon@chemistry.harvard.edu
The ORCID identification number(s) for the author(s) of this article can be found under https://doi.org/10.1002/adfm.202211338.

DOI: 10.1002/adfm.202211338

(abbreviated 2-2PEAQ). 2-2PEAQ is a singly substituted anthraquinone that is synthesized via a facile synthetic route from potentially inexpensive precursors (Table S1, Supporting Information). 2-2PEAQ has the lowest molecular weight (MW = 296.07 g mol^{-1}) among the anthraquinone derivatives reported previously that can deliver high stability (<0.02% per day fade rate), low membrane permeability (<1×10^{-13} cm^2 s^{-1} using Nafion 212 (Nafion is a trademark polymer from DuPont)), high solubility (≥1 M transferrable electrons) and acceptable redox potential (OCV > ≈1.0 V versus $Fe(CN)_6^{3-/4-}$) for use in aqueous organic flow batteries (Table S2, Supporting Information). We extensively evaluated a battery based on 2-2PEAQ negolyte paired with ferri/ferrocyanide posolyte (cell voltage of 0.96 V), under different pH values, current densities, cut-off voltage values, and at a low concentration of 0.1 M as well as the high concentration of 1 M (equivalent to 2 M of transferrable electrons). We additionally employed a rejuvenation strategy to electrochemically recompose the original compound from one of the decomposition products, the anthrone derivative.[26] The compound is found to have a high stability of ≈0.03–0.05% per day under variety of operational conditions and an extremely high stability, with an overall residual fade rate of only 0.01% per day, with the electrochemical rejuvenation strategy. Additionally, our post-mortem analyses via mass spectrometry and NMR confirmed that anthrone formation and side chain loss had occurred during the operation. Because the compound has only one side chain, we could directly isolate the effect of the ether linkages attached on carbons non-adjacent to the central ring (the beta position) and adjacent to the central quinone ring (the alpha position) on the compound's stability without the complication arising from two separate side chains. Hence, we additionally synthesized and evaluated the alpha-substituted isomer of 2-2PEAQ (abbreviated 1–2PEAQ). 1–2PEAQ showed three times faster fade rate and lower solubility compared to 2-2PEAQ. Our results demonstrate a promising negolyte with attractive performance factors for a viable redox flow battery.

2. Results and Discussion

2.1. Half-Cell Electrochemical Characterization

A series of half-cell studies were conducted to characterize the electrochemical properties of 2-2PEAQ. **Figure 1**a shows the cyclic voltammetry of 5 mM 2-2PEAQ in a pH 14 solution of potassium hydroxide. The redox potential is −0.477 V versus SHE (E_{red} = −0.504 V vs SHE, E_{ox} = −0.449 V vs SHE) with a peak separation of 55 mV at 0.05 V s^{-1}, enabling a theoretical cell voltage of 0.957 V when paired with a ferrocyanide positive electrolyte (posolyte). Figure 1b demonstrates a slope of 60 mV pH^{-1} unit from pH 7.5 to pH 10.6, followed by a slope of 25 mV pH^{-1} unit from pH 10.8 to pH 13, indicating a transition from a $2H^+/2e^-$ process to a $1H^+/2e^-$ process. This is followed by a flat proton-decoupled electron transfer region when the pH is above 13. The compound was further analyzed by conducting rotating disk electrode measurements. The diffusion coefficient (D) of the oxidized 2-2PEAQ compound was determined by extracting the limiting current values under different rotation rates (Figure 1c) and the use of the Levich equation. The diffusion coefficient of the oxidized 2-2PEAQ compound found to be 2.23×10^{-6} cm^2 s^{-1} (Figure 1d), which is of the same order of magnitude as those of other redox active anthraquinones. Additionally, the kinetic information of the oxidized 2-2PEAQ was extracted by conducting Koutecký-Levich analysis. The reciprocal current at different overpotentials versus the reciprocal root of the angular rotation rate was plotted, which yielded a straight line (Figure 1e), an intercept of which was the reciprocal kinetic current ($1/j_K$). A plot of the logarithm of the kinetic current (j_k) versus overpotential was used to determine the rate constant (k^0) for the charge transfer of 2-2PEAQ (Figure 1f). The fitted Tafel plot yielded a rate constant of 1.75×10^{-3} cm s^{-1}, depicting the fast kinetic rates commonly observed for organic redox active species with the anthraquinone core structure.[21] Comparable results were found when the half-cell tests were conducted at the initial pH of 7 (Figure S1, Supporting Information).

2.2. Solubility

The solubility limit of 2-2PEAQ is 1.0 M at pH 14. This is equivalent to 2.0 M transferrable electrons at pH 14, resulting in a volumetric capacity of 53.6 Ah L^{-1} at this pH value. Note that the methyl group on the side chain increased the solubility of the compound. We found that without the methyl group, the solubility is <0.1 M. Our working hypothesis is that the methyl group frustrates crystal packing by decreasing the planarity of the molecule and creating a racemic mixture.

2.3. Polarization and Galvanostatic Analysis

We next conducted a polarization and galvanostatic analysis of a cell composed of high concentration (1 M 2-2PEAQ) at elevated temperature. **Figure 2**a depicts an increase in the open circuit voltage (OCV) of the battery from 0.965 V at 20% SOC to 1.05 V at 80% SOC. The high frequency area-specific resistance (ASR) of the battery is averaged to 2.3 Ω cm^{-2} across all SOC ranges. The average polarization ASR is 3.0 Ω cm^{-2}, which indicates that 77% of the total resistance of the cell is attributed to the membrane resistance in the system. The peak power density at 50% SOC is found to be 87.2 mW cm^{-2}. The noise depicted in Figure 2b is caused by the pulsation of the peristaltic pump used for the operation of the cell at high concentrations, causing momentary depletion of the electrolyte and mass transfer limitations. Polarization tests were also conducted at low concentration of ≈4.7 mL 0.1 M 2-2PEAQ in 1 M KOH paired with 50 mL of 0.1 M ferrocyanide/0.02 M ferricyanide in 1 M KOH and at room temperature (Figure S2, Supporting Information), equally showing large contributions of membrane to the overall cell ASR. Note that Figure S3 (Supporting Information) demonstrates that replacing the Nafion 212 with Fumasep E620 significantly reduces the battery ASR, demonstrating that another commercially available membrane would allow for better performance. The conductivity of the 0.1 M 2-2PEAQ electrolyte in 1 M KOH was found to be 0.163 S cm^{-1}, which is comparable to

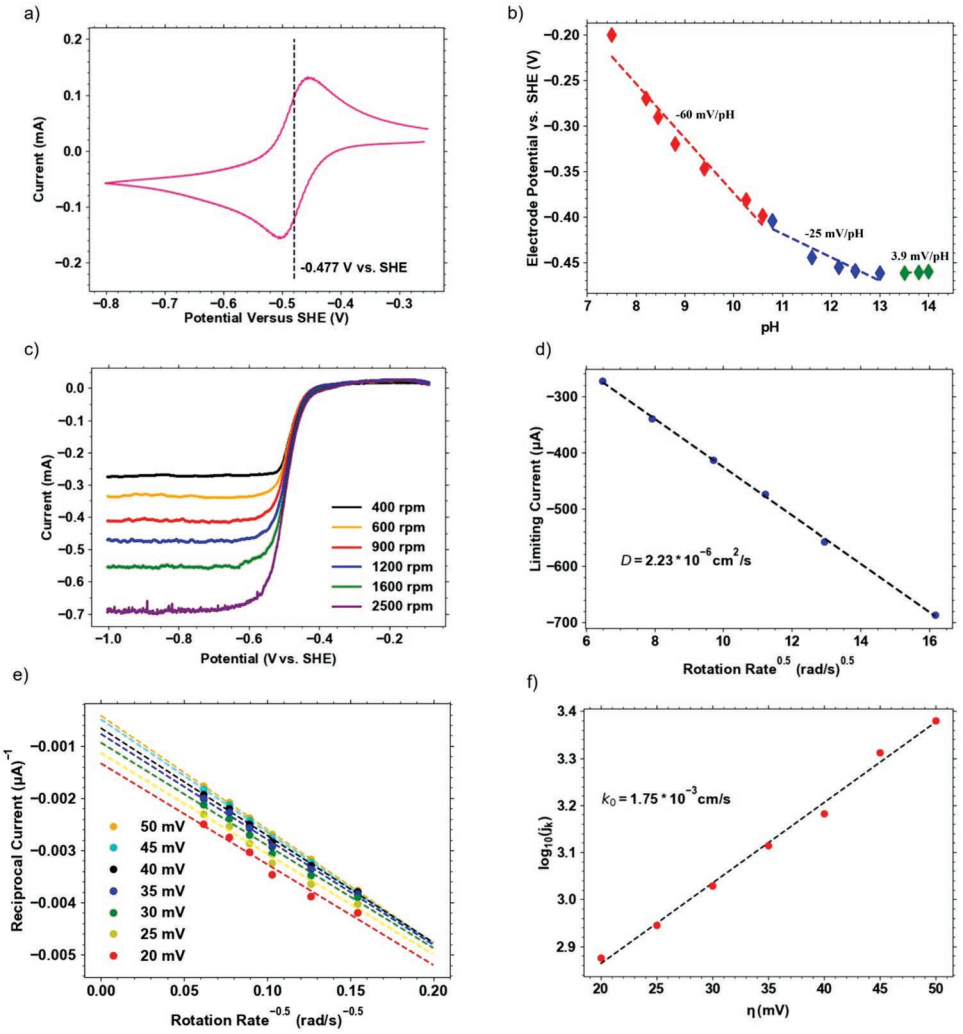

Figure 1. a) Cyclic voltammetry of 5 mM 2-2PEAQ in 1 M KOH with a scan rate of 50 mV s^{-1}. b) Pourbaix diagram of 5 mM 2-2PEAQ. Rotating-disk-electrode experiment on 5 mM 2-2PEAQ in 1 M KOH solution. c) Linear sweep voltammograms on a glassy carbon rotating disk electrode at rotation rates between 400 and 2500 rpm with potential sweeping rate of 20 mV s^{-1}. d) Levich plot of limiting current versus square root of rotation rate. e) Koutecký–Levich plot of 5 mM 2-2PEAQ in 1 M KOH solution at different overpotentials. f) Fitted Tafel plot of 5 mM 2-2PEAQ in 1 M KOH.

0.193 S cm^{-1} found for 0.1 M 2,6-dihydroxyanthraquinone (2,6–DHAQ) in 1 M KOH.

In order to extract the accessed capacity and resulting round-trip efficiencies at different applied current densities, purely galvanostatic measurements was conducted. Increased voltage loss due to ohmic resistance at higher applied current densities resulted in lower accessed capacity and lower round-trip voltage efficiency as demonstrated in Figure 2c,d, respectively. As can be seen in Figure 2d, the majority of loss in the energy efficiency is rooted in voltage efficiency loss. The slight drop in the coulombic efficiency is the result of simultaneous effect of mass transfer limitations during discharge and higher voltage loss due to ohmic resistances at higher applied current densities. Mass transfer during discharge depends on the concentration of the reduced species that is formed during the charging process. At higher applied current densities, due to ohmic resistances, lower concentration of reduced species is formed (lower accessed capacity at high currents as shown in Figure 2c), hence mass transfer overpotential sets in earlier during the discharge, preventing one to convert back all the reduced species. Mass transfer overpotential during the charging process is lower compared to the discharge because the total bulk concentration is available for the reaction. Similar trends were found when galvanostatic tests were conducted at the low concentration of 0.1 M 2-2PEAQ and at room temperature (Figure S2, Supporting Information). Note that in these tests, after each constant current charge/discharge test, we ensured that the battery was completely discharged by conducting a constant current followed by constant voltage (CCCV) discharge step (not shown). This would bring back the battery to 0% SOC for the next constant current test. In the absence of this discharge step, the decrease in the coulombic efficiency is less pronounced (Figure S4, Supporting Information), because the reduced concentration would accumulate, masking the real mass transfer overpotentials.

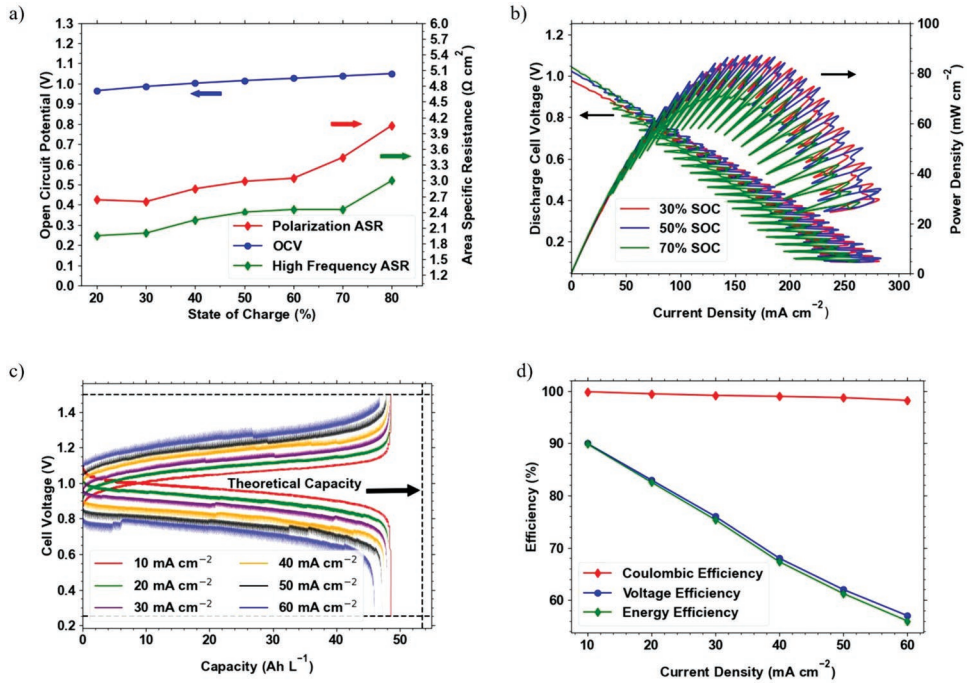

Figure 2. Polarization and galvanostatic performance of a cell composed of ≈5 mL of 1 M 2-2PEAQ in 1 M KOH and 100 mL of 0.3 M ferrocyanide (potassium salt)/0.2 M ferrocyanide (sodium salt)/0.3 M ferricyanide (potassium salt) (13.4 Ah L^{-1}) in 1 M KOH separated by a Nafion 212 cation exchange membrane at elevated temperature of 40 °C. The cell cycling tests were conducted in a N_2-filled glove box. The capacity is presented in units of Ampere-hours per liter of negolyte. a) Plots of OCV and high frequency and polarization ASR versus SOC. b) Cell voltage and power density during discharge at selected SOCs. c) Galvanostatic charge-discharge curves at various current densities with 1.5 and 0.25 V cutoffs. The theoretical capacity is indicated by the vertical dashed line. d) Coulombic, voltage, and energy round-trip efficiencies at different applied current densities.

2.4. Long-Term Battery Performance

The long-term cycling tests were conducted at two different pH values. First, a battery composed of 0.1 M 2-2PEAQ in 1 M KCl paired with 0.1 M ferrocyanide/0.02 M ferricyanide in 1 M KCl was cycled with CCCV protocol at 40 mA cm^{-2} with voltage cut-off values of 1.3 and 0.5 V. **Figure 3**a depicts the charge and discharge capacities and the coulombic efficiencies over the span of 10 days of operation. The coulombic efficiency was at ≈100% over the entire 10 days of operation. The theoretical accessible capacity based on 0.1 M concentration of 2-2PEAQ is 5.36 Ah L^{-1} and the accessed capacity in practice was 83% at pH 7 and 93% at pH 14. The difference between realized capacity and the theoretical value could come from errors in electrolyte volume measurement or the presence of redox-inactive impurities. The temporal fade rate of the 2-2PEAQ at pH 7 was 0.09% per day, demonstrating a high stability. The voltage–capacity profiles of this battery at three selected cycle numbers are shown in Figure 3b.

Next a battery composed of 0.1 M 2-2PEAQ at pH 14 was cycled with the same protocol as that described for the pH 7 experiment. Note that the given compound is proton-coupled at pH 7 (Figure 1b), pH swing occurs during cell cycling,[25] As shown in Figure 3c, the coulombic efficiency similarly remained at ≈100% over the span of 10 days. A significantly lower temporal fade rate of 0.05% per day at pH 14 is achieved, demonstrating an excellent cycling stability and performance at pH 14. The excellent chemical stability of the compound can also be confirmed from the NMR spectra taken before and after a thermal stability test on both the reduced and oxidized 2-2PEAQ (at pH 14) in the absence of cell cycling. The NMR spectra of 2-2PEAQ before and after heating the samples for 1 week at 65 °C in both the oxidized and the reduced form can be found in Figure S5 (Supporting Information). No new peaks were observed in either post-heating NMRs, indicating the 2-2PEAQ is resistant to thermal decomposition on the time-scale studied.

In order to analyze the decomposition product of 2-2PEAQ during the cell cycling at pH 14, the cycled electrolyte was further investigated by CV, NMR, and liquid chromatography. Cyclic voltammogramms of both the negolyte and the posolyte reservoirs were performed without dilution (Figure S6, Supporting Information) and showed no sign of crossover of ferrocyanide into the negolyte or 2-2PEAQ into the posolyte. No unexpected peaks were seen on either ^{13}C NMR (Figure S7, Supporting Information) or the proton NMR of ferrocyanide (Figure S8, Supporting Information). This is consistent with the lack of observable crossover seen in cyclic voltammetry studies. The proton NMR spectrum of the post cycled compound (stopped at its fully oxidized form) reveals new peaks in the aromatic region immediately up field of the original 2-2PEAQ peaks (Figure S9, Supporting Information). These new peaks are ≈10% the size of the peaks corresponding to 2-2PEAQ. The new aromatic peaks were identified as belonging to 2-hydroxyanthraquinone. The formation of 2-hydroxyanthraquinone demonstrates a decomposition mechanism by side-chain loss. A new peak is observed in the aliphatic region as a singlet at 1.87 (Figures S9 and S10, Supporting Information),

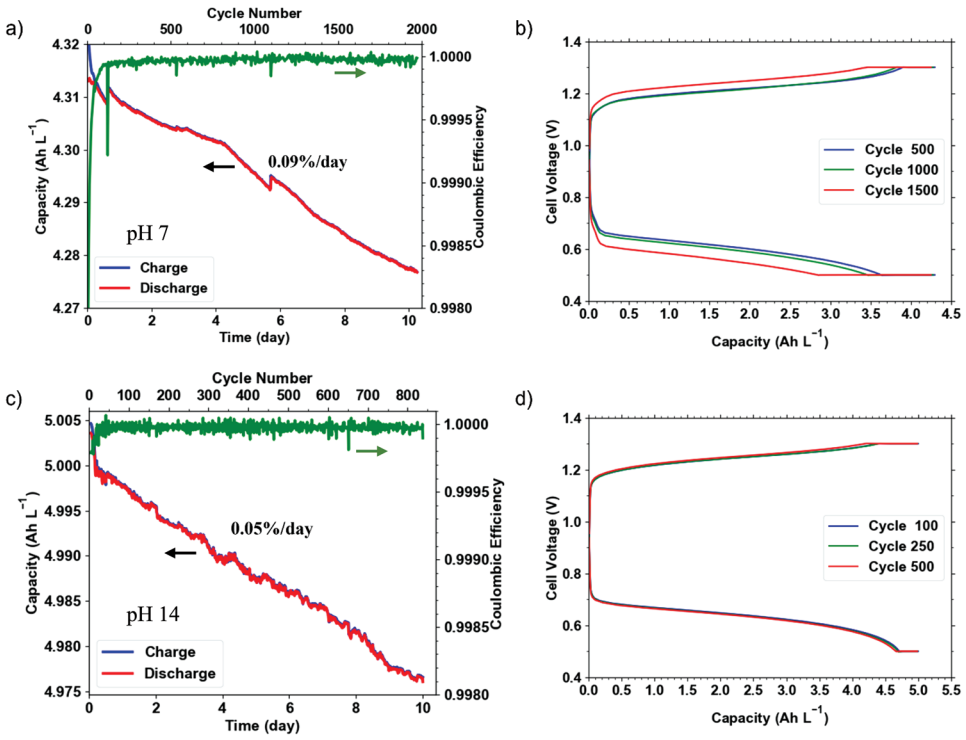

Figure 3. Long term cell cycling of flow batteries at initial pH of 7 a,b) and pH 14 c,d) operated with a constant current (40 mA cm^{-2}) followed by constant potentials of 1.3 V (charging) and 0.5 V (discharging) during 10 days of operation at room temperature. The cell was assembled with 0.1 M 2-2PEAQ in 1 M KCl (for pH 7) or 1 M KOH (for pH 14) paired with 50 mL of 0.1 M ferrocyanide/0.02 M ferricyanide in 1 M KCl (for pH 7) or 1 M KOH (for pH 14) separated by a Nafion 212 cation exchange membrane. The cell cycling tests are conducted in a N_2-filled glove box. The capacity is presented in units of Ampere-hours per liter of negolyte. a) Charge and discharge capacities and coulombic efficiency versus time at pH 7 b) Charge–discharge voltage-capacity profiles of 2-2PEAQ from selected cycles in (a). c) Charge and discharge capacities and coulombic efficiency versus time at pH 14 d) Charge–discharge voltage–capacity profiles of 2-2PEAQ from selected cycles in (c).

which we believe belongs to the potassium pyruvate side chain. No peaks corresponding to the peaks expected of potassium lactate, potassium acrylate, or their decomposition products, at the same pH (Figures S10 and S11, Supporting Information) were detected. The side chain loss mechanism is expected to result in production of lactic acid. The proposed presence of pyruvic acid suggests that the further oxidation of lactic acid to pyruvic acid might occur rapidly. Furthermore, post-cycling LC-MS (Figure S12, Supporting Information) on both the cycled posolyte and negolyte solutions were conducted. The LC-MS results verified the presence of 2-hydroxyanthraquinone in the negolyte solution after cycling, consistent with the post-cycling NMR spectrum. Additionally, 2-hydroxyanthraquinone was also observed in the posolyte, but no intact 2-2PEAQ was observed – suggesting that the side chain slows crossover of this molecule through the membrane. From this post-cycling analysis, we conclude that the side chain loss has contributed to the degradation of 2-2PEAQ during the cell cycling.

A second degradation mechanism commonly seen for anthraquinone is the anthrone formation and formation of anthrone dimer. The presence of dimer or anthrone would not be detected in the above post-cycling analysis due to the presence of air during NMR and LC-MS experiments, which oxidizes any anthrone or anthrone dimer that might have formed. To investigate the formation of the anthrone derived from 2-2PEAQ, we conducted an acidification procedure described in the Experimental Section. Our stacked NMR spectra (Figure S13, Supporting Information) in combination with the mass spectrometric data from the treated 2-2PEAQ (Figure S14, Supporting Information) clearly support the formation of anthrone, which can be recovered back to 2-2PEAQ both chemically and electrochemically. Formation of anthrone is also consistent with the lower fade rate achieved during the cell cycling at higher pH (Figure 3). The anthrone formation reaction also creates hydroxide; therefore, raising the hydroxide concentration in the electrolyte cuts the thermodynamic driving force for anthrone formation.[22]

We further analyzed the stability of 2-2PEAQ in the presence of lactic acid that is to be formed after the side chain loss (see the Experimental Sections for details). We found the disappearance of aromatic proton peaks of 2-2PEAQ after 30 min of the experiment (Figure S15, top, Supporting Information), and the same sample had a signal at 3506 G in EPR spectroscopy (Figure S16, Supporting Information). These data strongly indicate the formation of semiquinone radical species of 2-2PEAQ, likely through single electron transfer from deprotonated lactic acid to 2-2PEAQ under alkaline conditions. Thermal treatment of the sample at 45 °C for a week generated the new chemical species ≈6.2–8.6 ppm in ^{1}H NMR (Figure S15, bottom, Supporting Information). Semiquinone radical dimer and anthrone were detected by high-resolution LC–MS from the sample (Figure S17, Supporting Information). Thus, presence of lactic

acid in the negolyte could cause the generation of 2-2PEAQ semiquinone radical and its dimerization, albeit the concentration of lactic acid in the negolyte might be low.

We additionally investigated the cell cycling performance of the alpha-substituted isomer of 2-2PEAQ (abbreviated 1–2PEAQ) to understand the potential effect of the substituent position on the structural stability. A previous study of 1,2-DBEAQ and 1,8-DBEAQ isomers[27] found that the isomer with an ether linkage only on the carbon adjacent to the central quinone ring (the alpha carbon) experienced higher fade rates than the isomer with the linkage attached on carbons non-adjacent to the central ring (the beta position). Because 2-2PEAQ and 1–2PEAQ each have only one side chain, we could directly isolate the effect of alpha substituted and beta substituted ether-linked chain on the compound's stability without the complication arising from two separate side chains. 1–2PEAQ possesses a redox potential of –0.49 V versus SHE (Figure S18, Supporting Information), which is close to that of 2-2PEAQ. Thermal stability tests (Figure S19, Supporting Information) and consequently, cell test with a battery composed of 0.1 M 1–2PEAQ in 1 M KOH paired with 0.1 M ferrocyanide/0.02 M ferricyanide in 1 M KOH was conducted. 1–2PEAQ exhibited a fade rate of 0.16% per day (Figure S20, Supporting Information), which is three times that of 2-2PEAQ. The 1-position functionalization can facilitate the intramolecular nucleophilic substitution reaction between the carboxylate anion and the 1-position carbon which further accelerates the hydrolysis and causes irreversible chain cleavage. This is consistent with the previous theoretical calculations that showed 1-position substituted AQs are more thermodynamically susceptible to structural decomposition.[27] Additionally, the compound showed significantly lower solubility (0.13 M at pH 14) compared to 2-2PEAQ. Based on our post-mortem analysis described in Figures S21–S23 (Supporting Information), we believe the same side chain loss mechanism occurs for the alpha-substituted isomer, albeit at a faster rate compared to the beta-substituted molecule.[27] The anthrone formation mechanism of the isomer 1–2PEAQ is not further analyzed, but we expect anthrone and dimer formation mechanisms to be present for the 1–2PEAQ isomer as well, similar to the 2-2PEAQ compound.

To further investigate the effect of current density on the stability of 2-2PEAQ, the same cell was operated at a higher current density of 100 mA cm^{-2} followed by a constant voltage protocol at 1.35 and 0.5 V until the current drops to 1 mA cm^{-2}. A higher cut-off charging voltage was chosen to ensure access of the full capacity. The same temporal capacity fade rate of 0.05% per day was achieved at the higher current density of 100 mA cm^{-2} (Figure S24a, Supporting Information), demonstrating no influence of the applied current density on the fade rate. A volumetrically unbalanced, compositionally symmetric cell was also constructed to investigate the stability of the compound in the absence of the possible contributions from crossover. This cell cycling resulted in a slightly lower fade rate of 0.04% per day, demonstrating the high stability of 2-2PEAQ molecule (Figure S24b, Supporting Information). Note that our permeability experiments (described in the Experimental Section) show an extremely low permeability of the 2-2PEAQ through Nafion 212. Using the derivation of Fick's Law reported previously,[27] 2-2PEAQ permeability cannot exceed 1×10^{-13} cm^2 s^{-1} through Nafion 212 under the described experimental conditions.

We next investigated the possible effect of cut-off voltage values on the capacity fade rate of 2-2PEAQ. **Figure 4**a depicts the charge and discharge capacities and coulombic efficiency of the battery operated at a constant current of 40 mA cm^{-2} followed by constant charge and discharge voltage values shown, respectively, in Figure 4a. In every step, a tighter voltage window was employed successively, and the corresponding capacity fade rate was calculated. As can be seen, the fade rate drops to as low as 0.01% per day with the tightest voltage window of 0.55–1.2 V. The fade rate dependence on the cut-off voltage and whether its real or apparent[9] deserves further in-depth investigation. Employing a lower cut-off voltage window would naturally cause smaller accessed capacity during battery operation. In the present test, decreasing the cut-off voltage window from 0.5–1.3 V to 0.55–1.25 V results in 0.011 Ah L^{-1} lower accessed capacity, which is 0.22% of the total accessible capacity, a value that can commonly be assumed to be insignificant. However, in the context of highly stable compounds, this unutilized capacity can become significant, for example, for 2-2PEAQ with 0.05% per day temporal capacity fade rate, it would take 4.5 days to completely degrade 0.011 Ah L^{-1}, which should be considered if there exists a plausible root for the unutilized capacity to mask the real fade rate.

To further explore the possibility of achieving an even more stable performance, we employed the electrochemical recomposition strategy previously reported for DHAQ and AQDS compounds.[26] In this strategy, the anthrone and anthrone dimer formed over cycling are electrochemically converted back to anthraquinone derivatives by conducting a deep discharge step at a particular stage of operation. If anthrone formation has occurred during the cell cycling, we expect to be able to employ this method for recomposition of our compound.[28] Because 2-2PEAQ has a significantly lower fade rate compared to DHAQ (4–8% per day),[9] analysis of its recomposition is more attractive for practical applications. Figure 4b demonstrates the operation of the battery when a deep discharge step was repeated three times and, as can be seen after each deep discharge cycle, part of the faded capacity, which corresponds to the anthrone formed, was recovered. The recovery steps and the percentage recovered are shown in Figure S25 (Supporting Information). Taking the initial capacities after each recovery step for the capacity fade calculation yields an overall residual capacity fade rate of 0.01% per day. This is five times lower than the initial capacity fade rate of 0.05% per day and demonstrates that the 2-2PEAQ electrolyte has extremely stable capacity when rejuvenation is employed.[9]

Given the high stability of the 2-2PEAQ compound, we next conducted a cell study at a high concentration of 1.0 M, which is attractive for practical applications. **Figure 5**a shows the charge and discharge capacities and coulombic efficiency of a cell assembled by pairing the ≈5 mL 1 M 2-2PEAQ in 1 M KOH with 100 mL of 0.3 M ferrocyanide (potassium salt)/0.2 M ferrocyanide (sodium salt)/0.3 M ferricyanide (potassium salt). A mixture of potassium and sodium salts is used on the positive side to increase the solubility of ferrocyanide. As can be seen in Figure 5a, the compound remains highly stable with a capacity fade rate of 0.03% per day at 1.0 M, with very similar

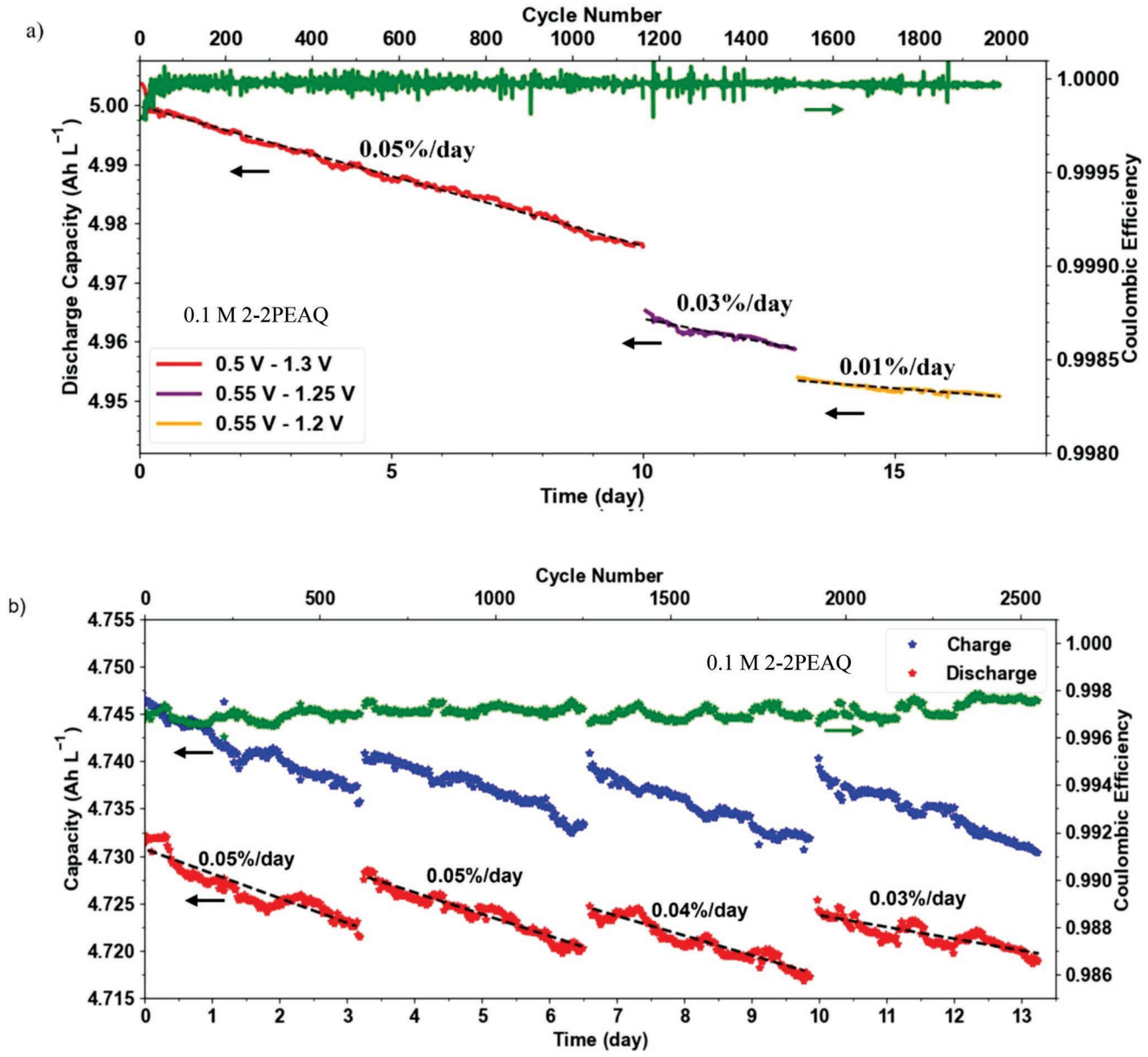

Figure 4. a) Effect of cut-off voltage on the long-term cell cycling of a flow battery assembled with 0.1 M 2-2PEAQ in 1 M KOH paired with 50 mL of 0.1 M ferrocyanide/0.02 M ferricyanide in 1 M KOH separated by a Nafion 212 cation exchange membrane operated at constant current of 40 mA cm^{-2} and at room temperature. b) Regeneration of the decomposed 2-2PEAQ by conducting a deep discharge step after every ≈3 days of operation.

voltage–capacity profiles over many cycles as can be seen in Figure 5b. The theoretical capacity of 1.0 M 2-2PEAQ (2.0 M electron transfer) is 53.6 Ah L^{-1}, and the practical accessed capacity in this test was 92%. Note that the previous cell cycling tests were conducted at room temperature and it is anticipated that the elevated temperature would increase the rate of degradation. For such evaluation, after almost 9 days of operation at room temperature (Figure 5a), the temperature of the cell was elevated to 40 °C, and an accelerated degradation rate of 0.09% per day was found (Figure S26, Supporting Information).

Given the high stability of the compound at high concentrations, we conducted a rejuvenation study at this concentration for 2-2PEAQ as well. The 5 mL 1.0 M 2-2PEAQ solution (pH 14) that was used for the power density and galvanostatic experiments (shown in Figure 2) was brought to room temperature and operated for ≈20 cycles before the first recovery was conducted. The accessed capacity of the fresh solution (before conducting experiments shown in Figure 2) was 49.00 Ah L^{-1} (91.42% of the theoretical capacity) and the lost capacity during high temperature analysis was ≈1.1% (48.48 Ah L^{-1} remained). The first recovery brings back the capacity to 48.52 Ah L^{-1}. Then the battery was operated for ≈40–50 cycles before each deep discharge step. As shown in Figure 5c, the fade rate during each portion of operation was already extremely low at ≈0.01% per day–lower than the 0.03–0.05% per day fade rate we found previously for the 0.1 M concentration. The deep discharge steps for

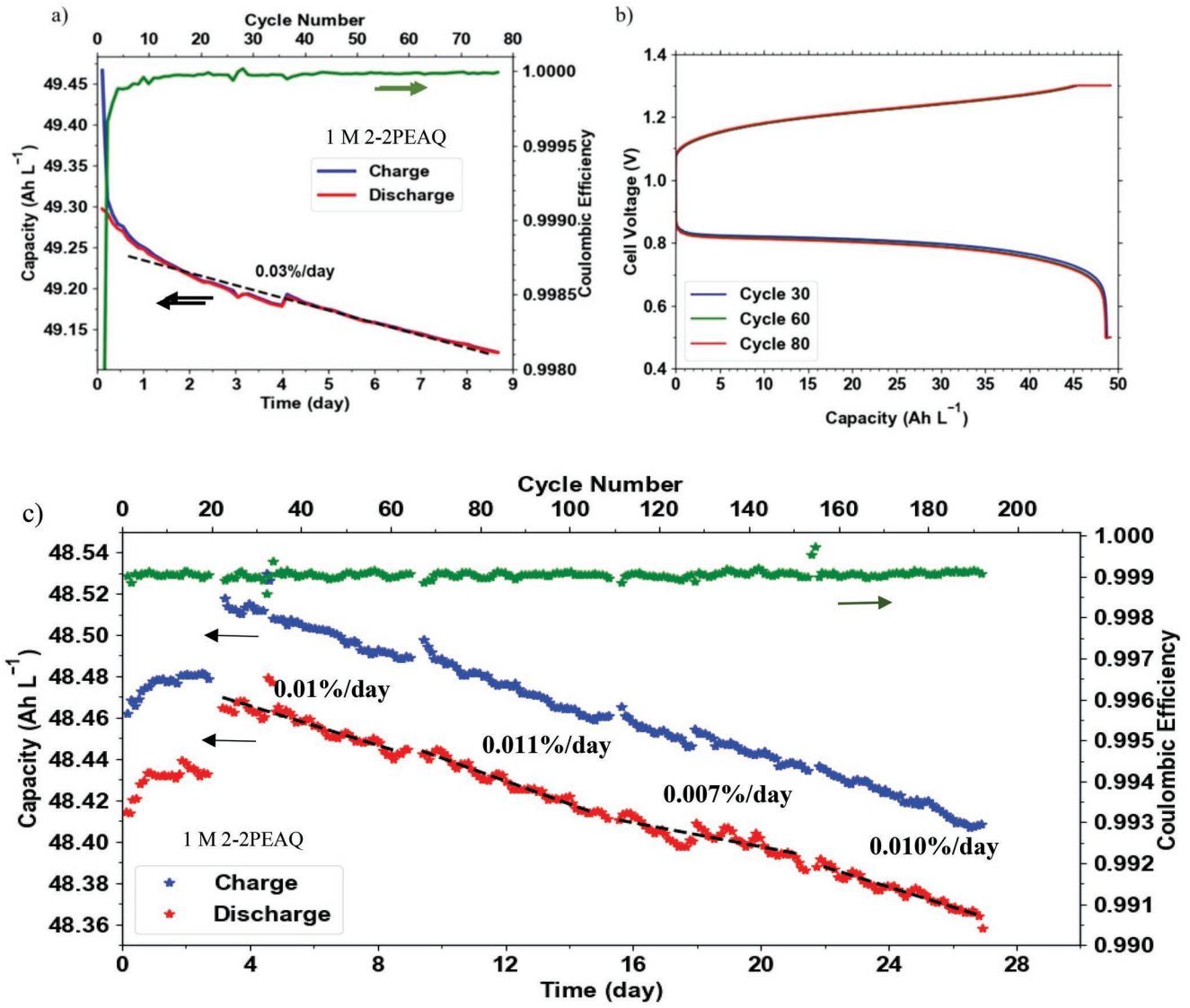

Figure 5. Long term cell cycling of a flow battery composed of ≈5 mL 1 M 2-2PEAQ in 1 M KOH (53.6 Ah L^{-1} capacity) paired with 100 mL of 0.3 M ferrocyanide (potassium salt)/0.2 M ferrocyanide (sodium salt)/0.3 M ferricyanide (potassium salt) (134 Ah L^{-1}) at room temperature. A constant current of 40 mA cm^{-2} followed by constant potentials of 1.3 V (charging) and 0.5 V (discharging) was employed. The cell cycling test is conducted in a N_2-filled glove box. The capacity is presented in units of Ampere-hours per liter of negolyte. a) Charge and discharge capacities and coulombic efficiency versus time b) Charge-discharge voltage-capacity profiles of 2-2PEAQ from selected cycles in a). c) Regeneration of the decomposed 2-2PEAQ by conducting a deep discharge step after every ≈40–50 cycles of operation.

this test did not result in recovery of a significant amount of lost capacity. Given that the rejuvenation strategy is effective in recovering the capacity lost only due to anthrone and dimer formation, this result suggests that the 0.01% per day fade rate found in this study is almost completely coming from the side chain loss mechanism, which is favored by the high pH. It seems that any anthrone formed was at too low of a concentration in this experiment for the recovery technique to yield noticeable results. Taking the initial capacities after each recovery step for the capacity fade calculation yields a slightly lower net capacity fade rate of 0.009% per day. This extremely low capacity fade rate combined with the high solubility of 2-2PEAQ would allow the construction of a practical energy-dense and stable organic-based redox flow battery for energy storage and conversion applications.

3. Conclusion

We introduced an extremely stable, energy-dense (53.6 Ah L^{-1}, 2 M transferrable electrons), low cross-over, and potentially inexpensive low molecular weight anthraquinone with the 2-2-propionate ether anthraquinone structure (abbreviated 2-2PEAQ) for use in redox flow batteries. The performance of the compound was rigorously studied at pH 7 and pH 14 under different applied current densities, cut-off voltage windows, and concentrations (0.1 and 1.0 M). The compound demonstrated a high stability (fade rate 0.03–0.05% per day) under all tested conditions in a full cell as well as a symmetric cell. We identified two mechanisms of capacity fade – side-chain loss and the formation of electrochemically inactive anthrone

and its dimer. 2-2PEAQ showed an extremely high stability (fade rate 0.01% per day) when we employed an electrochemical electrolyte rejuvenation strategy, which recomposes the anthraquinone from the anthrone and its dimer, but does not reverse the side-chain loss. We additionally investigated its alpha-substituted isomer (1-2PEAQ) and found it has three times higher fade rate compared to the beta-substituted compound (2-2PEAQ). Post-mortem analysis (NMR, mass spectroscopy and CV) demonstrated two degradation mechanisms; side chain loss, and anthrone formation. The present study introduces an extremely stable and energy-dense negolyte candidate whose performance was scrutinized under practically relevant conditions, advancing the prospects for commercialization of grid-scale aqueous organic redox flow batteries.

4. Experimental Section

Rotating Disk Electrode (RDE): The electrochemical properties of 2-2PEAQ were determined by rotating disk electrode (RDE) tests. The RDE tests were performed using a Pine Instruments Modulated Speed Rotator AFMSRCE equipped with a 5 mm diameter glassy carbon working electrode (Pine Instruments E5PK), an Ag/AgCl (3 M KCl) reference electrode (CHI), a graphite counter electrode and a Gamry Reference 3000 potentiostat.

Solubility Tests: Saturated solutions of 1–2PEAQ and 2-2PEAQ were prepared by first adding the respective salts to KOH electrolytes and adjusting the pH until precipitation was visible and the pH of each sample was 14. Each sample was stirred, sonicated for 30 min, and then left quiescent overnight. When precipitates were still visible and the pH remained 14 the next day, the solutions were filtered with a 0.2 µm syringe filter (VWR) and their concentrations were measured with UV–vis spectrophotometry (Agilent).

Polarization and Galvanostatic Tests: Polarization and galvanostatic experiments were conducted for low and high concentrations and temperatures. For low concentration tests, a cell composed of ≈4.7 mL 0.1 M 2-2PEAQ (96 C theoretical capacity) in 1 M KOH (1.1 M KOH was added initially for deprotonation of 0.1 M 2-2PEAQ) paired with 50 mL of 0.1 M ferrocyanide/0.02 M ferricyanide (482 C theoretical capacity) in 1 M KOH was prepared and tested at room temperature. For high concentration tests, a cell composed of ≈5 mL 1 M 2-2PEAQ in 1 M KOH (965 C theoretical capacity) paired with 100 mL of 0.3 M ferrocyanide (potassium salt)/0.2 M ferrocyanide (sodium salt)/0.3 M ferricyanide (potassium salt) (4824 C) in 1 M KOH was prepared and tested at 40 °C. Because it was expected that under conditions of practical deployment, self-heating would lead to elevated operating temperatures, the elevated temperature of 40 °C and high concentration of 1.0 M were used to show the achievable peak power density when mass-transfer limitations were improved at high temperature and concentration. In both cases, excess capacity was used in the posolyte to ensure that the negolyte side with 2-2PEAQ was the capacity limiting side of the cell. The two half-cells were separated by a Nafion 212 cation exchange membrane pretreated in 1 M KOH solution for at least overnight. 3 layers of carbon paper (SGL 39AA) baked at 400 °C overnight were used in each half-cell.

To prepare polarization plots for different states of charge, the full accessed capacity of the cell was first determined by a complete charge/discharge cycling conducted by applying a 40 mA cm^{-2} constant current followed by potential holds at 1.3 V (charge) and 0.5 V (discharge) until the current dropped to 1 mA cm^{-2}. The battery was then charged to different states of charges (calculated from the percentage of the complete accessed capacity) with 10% SOC intervals. At each SOC, electrochemical impedance spectroscopy (EIS) measurements were conducted with 10 mV perturbation and with frequency ranging from 1 to 100 000 Hz to find the high-frequency area-specific resistance (ASR). Additionally, the open–circuit voltage (OCV) of the battery was measured. Furthermore, at each SOC, the potential was swept from 1.0 to 0 V at a scan rate of 150 mV s^{-1} and the resulting current response was measured for generating polarization curves. The linear region of the polarization curves between 0.9 and 0.8 V was used to calculate the polarization ASR.

For purely galvanostatic tests, constant current densities between 10 and 60 mA cm^{-2} with intervals of 10 mA cm^{-2} were applied during both charge and discharge cycles without potential holds. Cut-off values of 1.5 and 0.25 V were used. Consequently, the coulombic, voltage, and energy efficiencies were calculated for each current density. Note that after each constant current density test, the battery was completely discharged by conducting a CCCV protocol and then the next constant current density was employed. This procedure was done to ensure that for every test, the battery charge/discharge cycling had begun from the same initial condition (0% SOC), making the comparison accurate.

Prolonged Cell Cycling Tests: Multiple long-term cell tests were conducted at different operational conditions to evaluate the cycling performance of 2-2PEAQ negolyte. All cycling tests were conducted by employing the constant current followed by constant voltage (CCCV) protocol. For the pH 7 study, a cell composed of ≈5 mL 0.1 M 2-2PEAQ in 1 M KCl (96 C theoretical capacity) paired with 50 mL of 0.1 M ferrocyanide/0.02 M ferricyanide (482 C theoretical capacity) in 1 M KCl was prepared. Note that excess capacity was used in the posolyte to ensure that the negolyte side with 2-2PEAQ was the capacity limiting side of the cell. If a capacity-balanced, osmotically balanced cell were to be designed with 2-2PEAQ and ferrocyanide, two to three times higher volume would have been needed on the ferrocyanide side. The need for dissymmetric volumes was rooted in the high number of dissociated ions of dissolved ferrocyanide and ferricyanide salts compared to 2-2PEAQ and other anthraquinone derivatives. Developing highly soluble, stable posolytes with matching ionic strength to 2-2PEAQ and other anthraquinone derivatives was an attractive option for further advancement of anthraquinone-based RFBs.

The two half-cells were separated by a Nafion 212 cation exchange membrane pretreated in 1 M KCl solution for at least overnight. Three layers of carbon paper (SGL 39AA) baked at 400 °C overnight were used in each half-cell. In all tests, a flow rate of 60 mL min^{-1} was used. The cell was cycled at a constant current of 40 mA cm^{-2}, followed by a constant charging voltage of 1.3 V and discharging voltage of 0.5 V until the current drops to 1 mA cm^{-2}. For the pH 14 tests, an alternative electrolyte of ≈5 mL 0.1 M 2-2PEAQ in 1 M KOH (96 C theoretical capacity) paired with 50 mL of 0.1 M ferrocyanide/0.02 M ferricyanide (482 C theoretical capacity) in 1 M KOH was employed. For the pH 14 tests, different cut-off voltage values were explored, which was stated in the related plots for each individual test. The same battery and electrolyte were then used for the rejuvenation study. In this study, the battery was operated at a constant current of 40 mA cm^{-2}, followed by a constant charging voltage of 1.3 V and discharging voltage of 0.5 V until the current drops to 1 mA cm^{-2}. After every ≈3 days, an additional discharge step of –0.05 V was conducted to recompose the oxidized 2-2PEAQ species from any anthrone that had possibly formed.

For conducting a comparison between the cell performance of 2-2PEAQ and 1–2PEAQ, a cell composed of ≈5 mL 0.1 M 1–2PEAQ (isomer) in 1 M KOH (96 C theoretical capacity) paired with 50 mL of 0.1 M Ferrocyanide/0.02 M Ferricyanide (482 C theoretical capacity) in 1 M KOH was prepared and operated at a constant current of 40 mA cm^{-2}, followed by a constant charging voltage of 1.3 V and discharging voltage of 0.5 V until the current dropped to 1 mA cm^{-2}.

To explore the effect of current density, a test at pH 14 with a higher current density of 100 mA cm^{-2} (followed by a constant charging voltage of 1.35 V and discharging voltage of 0.5 V until the current dropped to 1 mA cm^{-2}) was also conducted.

For the symmetric cell test, a cell composed of ≈4 mL 0.1 M 2-2PEAQ in 1 M KOH (77 C theoretical capacity) (at 50% SOC) paired with 16 mL of 0.1 M 2-2PEAQ in 1 M KOH (at 50% SOC) was prepared. A constant voltage of ± 0.2 V is applied during each charge/discharge step, respectively, until the current drops to 1 mA cm^{-2}.

For the high concentration test, a cell composed of ≈5 mL 1 M 2-2PEAQ in 1 M KOH (964 C theoretical capacity) paired with 100 mL of 0.3 M ferrocyanide (potassium salt)/0.2 M ferrocyanide (sodium salt)/0.3 M ferricyanide (potassium salt) (4824 C) was constructed. Excess capacity was used in the posolyte to ensure that the negolyte side with 2-2PEAQ was the capacity limiting side of the cell. For the recomposition study at high concentration, the same battery and electrolytes used for the high concentration polarization and galvanostatic tests were employed. In this study, the battery was operated at a constant current density of 40 mA cm^{-2}, followed by a constant charging voltage of 1.3 V and discharging voltage of 0.5 V until the current density dropped to 1 mA cm^{-2}. After every ≈40–50 cycles, an additional discharge step with lower discharge voltage was conducted. For three of these recovery steps a discharge voltage of −0.05 V and for one of the steps a discharge voltage of 0.1 V was applied to recompose the oxidized 2-2PEAQ species from any anthrone that had possibly formed

ESI-MS and NMR Measurements: Samples were diluted with HPLC grade water to 20 µM. High-resolution LC-MS analysis was performed in the Small Molecule Mass Spectrometry Facility at Harvard University on a MiniLIMS. The elution solution was 0.1% v/v formic acid in acetonitrile. The ESI mass spectrum was recorded in positive ionization mode. Proton and carbon NMRs were obtained on a Bruker AVANCE NEO400 MHz instrument.

Permeability Experimental Section: UV–vis absorbance spectra were measured with an Agilent 8453 spectrophotometer. The glass H-cells were custom made by Adams & Chittenden scientific glassware. The Nafion NR212 ion was exchanged to potassium form by soaking for over 12 h at ambient temperature in 1 M KOH, prior to experiments. The H-cell donating compartment contained 10 mL of 0.1 M anthraquinone (either 1–2PEAQ or 2-2PEAQ) in 1 M KOH and the receiving compartment contained 10 mL of 0.1 M KCl in 1 M KOH. The electrolyte in the receiving compartment was designed to balance the pH and total number of ions in solution in the donating compartment, to minimize water crossover. The donating and receiving compartments were both stirred continuously using magnetic stir bars.

For each anthraquinone chemistry, three identical H-cells stirred for 14 days, and 2 mL samples were periodically taken from the receiving side to measure absorbance spectra and replaced with pristine receiving solution. The mass of solution in all H-cell receiving compartments changed by <2% over the course of the experiment.

An upper limit on permeability for each species was assigned based on the highest absorbance value observed at 337 nm for 2-2PEAQ or 380 nm for 1–2PEAQ in any of the replicate H-cells over the course of the 14-day experiment. This was done because the measured receiving side absorbance spectra did not match the peaks characteristic for the anthraquinones, and did not necessarily increase with time, indicating that the absorbance represented minor impurities in the system instead.

Anthrone Detection Procedure: First, 0.115 M 2-2PEAQ negolyte at pH 7 was prepared, then it was chemically reduced to ≈100% SOC, and then the electrolyte was treated at 85 °C for 7 days. The aged electrolyte to protonate the anthraquinone derivatives (AQ) for precipitation was acidified. The isolated AQ precipitates were then redissolved in DMSO-d_6 and transferred into an air-tight J-Young NMR tube. The reason behind choosing to acidify the electrolyte and dissolve AQ in DMSO-d_6 rather than directly using D_2O for ^1H NMR measurements was that radicals always exist in ≈100% SOC electrolytes which frustrate NMR signals due to their paramagnetic feature, but can be well quenched through protonation, thus enabling to analyze the NMR spectra in its reduced state.

Analysis of 2-2PEAQ/Lactic Acid Mixture: To a 20 mL vial with a stir bar, 2-2PEAQ (0.2 mmol), NaOH (0.2 mmol), lactic acid (0.05 mmol, degassed prior to using), and 2.0 mL of 1 M NaOH aq. were added in glovebox. After stirring the sample for 30 min, 0.1 mL of the solution and 0.55 mL of D_2O were transferred into an air-tight J-Young NMR tube for following analysis: ^1H-NMR spectra were recorded before and after heating the J-Young NMR tube (Figure S14, Supporting Information). ^1H NMR sample before heating was analyzed by EPR spectroscopy (Figure S15, Supporting Information). After heating ^1H NMR sample at 45 °C for 7 days, high-resolution LC-MS analysis was recorded for the detection of side products from 2-2PEAQ (Figure S16, Supporting Information).

Synthesis of 2-2PEAQ: Five grams of 2-hydroxyanthraquinone (22.3 mmol) was added to a 100 mL pear bottomed flask. Ethyl 2-bromopropionate (3.75 mL) (29 mmol, 1.3 eq) and 7.5 g of potassium carbonate (54 mmol, 2.4 eq). This solution was stirred in 40 mL DMF at 80 °C for 3 h and then vacuum filtered to give the ester. Without further purification the ester was suspended in 30 mL of water and 30 mL of isopropanol with 7.5 g of potassium hydroxide (133 mmol 16 eq). This solution was stirred at 80 °C for 3 h before being precipitated out using 1 M HCl as a green solid. Yield: 2.4 g (52.9%).

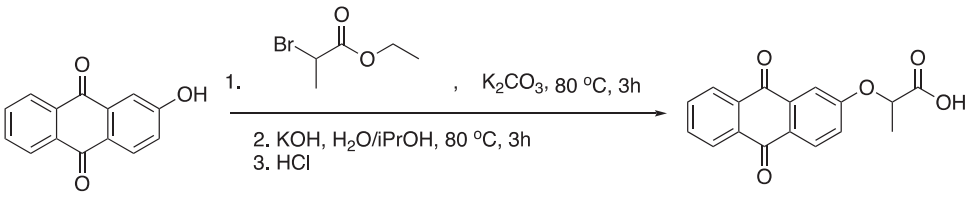

2,2-PEAQ

The stability of 2-2PEAQ was determined by taking NMR spectra before and after heating the sample for 1 week at 65 °C in both the oxidized and the reduced form. Following heating, the reduced form was oxidized by agitating the solution in ambient air for 30 min. 100 µL samples of each sample were separately diluted with 500 µL of D_2O before obtaining the spectra.

Synthesis of 1–2PEAQ: In 20 mL DMF, 2 grams of 1-hydroxyanthraquinone (8.09 mmol) were mixed with 6 mL of ethyl 2-bromopropionate (46.2 mmol, 5.7 eq) and 3 g potassium carbonate (21.7 mmol or 2.68 eq) (was heated at 90 °C overnight followed by the addition of water to precipitate out the ester. This was followed without further purification by hydrolysis with 5 g KOH (89.3 mmol, 11.03 eq) in 15 mL of each water and isopropanol. This stirred for 3 h at 80 °C followed by precipitation with 1 M HCl to give a sandy orange solid. The yield was 2 g (75.8%).

The stability of 1–2PEAQ was determined by taking NMR spectra before and after heating the sample for 1 week at 65 °C in both the oxidized and the reduced form. Following heating, the reduced form was oxidized by agitating the solution in room air for 30 min. Hundred microliter samples of each sample were separately diluted with 500 µL of D_2O before obtaining the spectra.

Supporting Information

Supporting Information is available from the Wiley Online Library or from the author.

Acknowledgements

K.A. and E.F.K. contributed equally to this work. This research was supported by the National Science Foundation through grant

CBET-1914543 and by U.S. DOE award DE-AC05-76RL01830 through PNNL subcontract 535264. K.A. was supported in part through the Natural Sciences and Engineering Research Council of Canada (NSERC) Postdoctoral Fellowship (PDF) program [application number PDF – 557232 – 2021]. T.T. was supported by Japan Society for the Promotion of Science (JSPS) for the postdoctoral fellowship. The authors thank Jennifer Wang for mass spectrometry analysis. The authors also thank Eric Fell, Jordan Sosa, Dawei Xi, Daniel Pollack, Eliza Spear, and Jinxu Gao for valuable discussions.

Conflict of Interest

R.G.G. and M.J.A. acknowledge significant financial stakes in Quino Energy, Inc., which might profit from the results reported here. All other authors declare no conflict of interest.

Data Availability Statement

The data that support the findings of this study are available in the supplementary material of this article.

Keywords

aqueous organic flow systems, energy storage and conversion, redox flow batteries

Received: September 29, 2022
Revised: December 13, 2022
Published online:

[1] J. Rugolo, M. J. Aziz, *Energy Environ. Sci.* **2012**, *5*, 7151.
[2] Z. Zhu, T. Jiang, M. Ali, Y. Meng, Y. Jin, Y. Cui, W. Chen, *Chem. Rev.* **2022**, *122*, 16610.
[3] A. Z. Weber, M. M. Mench, J. P. Meyers, P. N. Ross, J. T. Gostick, Q. Liu, *J. Appl. Electrochem.* **2011**, *41*, 1137.
[4] B. R. Chalamala, T. Soundappan, G. R. Fisher, M. R. Anstey, V. V. Viswanathan, M. L. Perry, *Proc IEEE Inst Electr Electron Eng* **2014**, *102*, 976.
[5] M. Rychcik, M. Skyllas-Kazacos, *J. Power Sources* **1988**, *22*, 59.
[6] S. Corcuera, M. Skyllas-Kazacos, *Europ. Chem. Bull.* **2012**, *1*, 8822.
[7] X. Wei, W. Pan, W. Duan, A. Hollas, Z. Yang, B. Li, Z. Nie, J. Liu, D. Reed, W. Wang, *ACS Energy Lett.* **2017**, *2*, 2187.
[8] J. Noack, N. Roznyatovskaya, T. Herr, P. Fischer, *Angew. Chem., Int. Ed.* **2015**, *54*, 9776.
[9] D. G. Kwabi, Y. Ji, M. J. Aziz, *Chem. Rev.* **2020**, *120*, 6467.
[10] Q. Chen, Y. Lv, Z. Yuan, X. Li, G. Yu, Z. Yang, T. Xu, *Adv. Funct. Mater.* **2021**, *32*, 2108777.
[11] H. Fan, W. Wu, M. Ravivarma, H. Li, B. Hu, J. Lei, Y. Feng, X. Sun, J. Song, T. L. Liu, *Adv. Funct. Mater.* **2022**, *32*, 2203032.
[12] Y. Li, Z. Xu, Y. Liu, S. Jin, E. M. Fell, B. Wang, R. G. Gordon, M. J. Aziz, Z. Yang, T. Xu, *ChemSusChem* **2021**, *14*, 745.
[13] Z. Zhao, B. Zhang, B. R. Schrage, C. J. Ziegler, A. Boika, *ACS Appl. Energy Mater.* **2020**, *3*, 10270.
[14] W. Wu, J. Luo, F. Wang, B. Yuan, T. L. Liu, *ACS Energy Lett.* **2021**, *6*, 2891.
[15] E. S. Beh, D. De Porcellinis, R. L. Gracia, K. T. Xia, R. G. Gordon, M. J. Aziz, *ACS Energy Lett.* **2017**, *2*, 639.
[16] S. Pang, X. Wang, P. Wang, Y. Ji, *Angew. Chem., Int. Ed.* **2021**, *60*, 5289.
[17] J. Xu, S. Pang, X. Wang, P. Wang, Y. Ji, *Joule* **2021**, *5*, 2437.
[18] K. Lin, R. Gómez-Bombarelli, E. S. Beh, L. Tong, Q. Chen, A. Valle, A. Aspuru-Guzik, M. J. Aziz, R. G. Gordon, *Nat. Energy* **2016**, *1*, 16102.
[19] Z. Li, T. Jiang, M. Ali, C. Wu, W. Chen, *Energy Storage Mater.* **2022**, *50*, 105.
[20] Y. Ji, M. A. Goulet, D. A. Pollack, D. G. Kwabi, S. Jin, D. De Porcellinis, E. F. Kerr, R. G. Gordon, M. J. Aziz, *Adv. Energy Mater.* **2019**, *9*, 1900039.
[21] M. Wu, Y. Jing, A. A. Wong, E. M. Fell, S. Jin, Z. Tang, R. G. Gordon, M. J. Aziz, *Chem* **2020**, *6*, 1432.
[22] M. Wu, M. Bahari, Y. Jing, K. Amini, E. M. Fell, T. Y. George, R. G. Gordon, M. J. Aziz, *Batter Supercaps* **2022**, *5*, e202200009.
[23] Y. Jing, E. M. Fell, M. Wu, S. Jin, Y. Ji, D. A. Pollack, Z. Tang, D. Ding, M. Bahari, M.-A. Goulet, T. Tsukamoto, R. G. Gordon, M. J. Aziz, *ACS Energy Lett.* **2021**, *7*, 226.
[24] M. Wu, M. Bahari, E. M. Fell, R. G. Gordon, M. J. Aziz, *J. Mater. Chem. A* **2021**, *9*, 26709.
[25] S. Jin, Y. Jing, D. G. Kwabi, Y. Ji, L. Tong, D. De Porcellinis, M.-A. Goulet, D. A. Pollack, R. G. Gordon, M. J. Aziz, *ACS Energy Lett.* **2019**, *4*, 1342.
[26] Y. Jing, E. W. Zhao, M.-A. Goulet, M. Bahari, E. M. Fell, S. Jin, A. Davoodi, E. Jónsson, M. Wu, C. P. Grey, *Nat. Chem.* **2022**, *14*, 1103.
[27] D. G. Kwabi, K. Lin, Y. Ji, E. F. Kerr, M.-A. Goulet, D. De Porcellinis, D. P. Tabor, D. A. Pollack, A. Aspuru-Guzik, R. G. Gordon, *Joule* **2018**, *2*, 1894.
[28] Y. Jing, M. Wu, A. A. Wong, E. M. Fell, S. Jin, D. A. Pollack, E. F. Kerr, R. G. Gordon, M. J. Aziz, *Green Chem.* **2020**, *22*, 6084.